Focal Liver Lesion Detection and Characterization with Diffusion-weighted MR Imaging:

Comparison with Standard Breath-hold T2-weighted Imaging[1]

Tejas Parikh, MD
Stephen J. Drew, MD
Vivian S. Lee, MD, PhD
Samson Wong, MD
Elizabeth M. Hecht, MD
James S. Babb, PhD
Bachir Taouli, MD

Purpose: To retrospectively compare diffusion-weighted (DW) magnetic resonance (MR) imaging with standard breath-hold T2-weighted MR imaging for focal liver lesion (FLL) detection and characterization, by using consensus evaluation and other findings as the reference standard.

Materials and Methods: Approval for this retrospective HIPAA-compliant study was obtained from the institutional review board; informed consent was waived. Fifty-three consecutive patients (30 men, 23 women; mean age, 60.7 years) with at least one FLL of 1 cm or greater in diameter were evaluated. Two independent observers reviewed DW (*b* values of 0, 50, and 500 sec/mm^2) and T2-weighted images for FLL detection and characterization. Reference standard for diagnosis was obtained from consensus review by the two observers of DW, T2-weighted, and dynamic contrast material–enhanced images, pathologic data, and follow-up imaging results. Apparent diffusion coefficient (ADC) was measured for FLLs identified at consensus review. DW and T2-weighted images were compared for FLL detection and characterization by using a binary logistic regression model. Receiver operating characteristic curve analyses were conducted to evaluate the utility of ADC for diagnosis of malignancy.

Results: Two hundred eleven FLLs (136 malignant, 75 benign) were detected at consensus review. Overall detection rate (averaged for two observers) was significantly higher for DW (87.7%) versus T2-weighted (70.1%) imaging ($P < .001$). FLL characterization was not significantly different between DW (89.1%) and T2-weighted (86.8%) imaging ($P = .51$). ADCs of malignant FLLs were significantly lower than those of benign FLLs ($P < .001$). The area under the curve for diagnosis of malignancy was 0.839, with sensitivity of 74.2%, specificity of 77.3%, positive predictive value of 85.5%, negative predictive value of 62.3%, and accuracy of 75.3%, by using a threshold ADC of less than 1.60×10^{-3} mm^2/sec.

Conclusion: DW MR imaging was better than standard breath-hold T2-weighted imaging for FLL detection and was equal to breath-hold T2-weighted imaging for FLL characterization.

Supplemental material: *http://radiology.rsnajnls.org/cgi/content/full/2463070432/DC1*

[1] From the Department of Radiology, New York University Medical Center, 530 First Ave, MRI, New York, NY 10016. Received March 6, 2007; revision requested May 14; revision received June 21; accepted July 19; final version accepted September 17. Partially funded by an award received by T.P. from the Society of Body CT and MRI in 2006. **Address correspondence to** B.T. (e-mail: *bachir.taouli@med.nyu.edu*).

Accurate detection and characterization of focal liver lesions (FLLs) are important for treatment planning for patients with liver neoplasms such as hepatocellular carcinoma (HCC) and metastases. The size and number of lesions can affect therapy. For example, patients with limited resectable metastatic lesions may benefit from curative resection (1) and patients with fewer than three small HCCs are candidates for liver transplantation (2). Patients with more extensive disease should instead undergo transarterial chemoembolization, radiofrequency ablation, or systemic chemotherapy (3,4).

For FLL detection and characterization, magnetic resonance (MR) imaging relies on T1-weighted, T2-weighted, and dynamic gadolinium-enhanced T1-weighted imaging (5–7). Results of several studies (8–17) have shown that diffusion-weighted (DW) MR imaging can help characterize FLLs by enabling measurement of lesion apparent diffusion coefficient (ADC).

A limited number of studies (18–21) have been performed on the use of DW imaging for FLL detection. To the best of our knowledge, only two studies involved the direct comparison of DW imaging and T2-weighted imaging in terms of FLL detection (results showed improved detection with DW vs T2-weighted imaging in 49 FLLs) (18) or in terms of image quality (results showed comparable image quality with DW imaging by using small *b* values compared with that with T2-weighted imaging) (22). DW images with low *b* values are similar to T2-weighted black-blood images, in which background signal of vessels in the liver parenchyma is suppressed (18,22), while higher *b* values give diffusion information that helps with FLL characterization (14,15).

To our knowledge, there are no published studies on the combination of detection and characterization of FLLs with DW imaging by using low and higher *b* values and on the comparison of DW MR imaging with standard T2-weighted imaging for detection and characterization of FLLs.

Thus, the purpose of our study was to retrospectively compare DW imaging with standard breath-hold T2-weighted imaging for FLL detection and characterization, by using consensus evaluation and other findings as the reference standard.

Advances in Knowledge

- Diffusion-weighted (DW) MR imaging with a small *b* value (50 sec/mm^2) significantly improves the detection of focal liver lesions compared with standard breath-hold T2-weighted imaging: 87.7% versus 70.1% ($P < .001$).
- DW imaging significantly improves detection of small malignant lesions (diameter, 1–2 cm) compared with standard breath-hold T2-weighted imaging (78.5% vs 45.8%) ($P < .001$).
- Respiratory-triggered DW imaging has a significantly higher detection rate than breath-hold DW imaging (93.7% vs 84.3%) ($P = .032$).

Materials and Methods

Patients

This study was Health Insurance Portability and Accountability Act compliant. Approval for this retrospective study was obtained from our institutional review board. A waiver of informed consent was obtained.

Our MR imaging database was retrospectively queried to identify patients who underwent DW MR imaging of the liver between May 2005 and September 2005 and who had at least one FLL measuring at least 1 cm in maximum diameter. Patients who did not undergo DW imaging and/or had no FLL or had an FLL less than 1 cm were excluded ($n = 149$).

The final cohort included 53 patients (30 men, 23 women; mean age, 60.7 years; age range, 25–83 years). There were 24 patients with chronic liver disease (including chronic hepatitis and cirrhosis) related to chronic viral hepatitis C ($n = 16$), chronic viral hepatitis B ($n = 5$), viral hepatitis B and C ($n = 2$), and alcohol abuse ($n = 1$). There were 13 patients with history of primary malignancy (colon cancer [$n = 3$], pancreatic cancer [$n = 3$], breast cancer [$n = 3$], gastric cancer [$n = 1$], malignant neuroendocrine tumor of the pancreas [$n = 1$], ovarian cancer [$n = 1$], and acute myelogenous leukemia [$n = 1$]). There were 16 patients with no history of chronic liver disease or malignancy who underwent MR imaging for evaluation of presumably benign FLL.

MR Imaging

MR imaging of the liver was performed by using different 1.5-T clinical systems (Magnetom Avanto, Sonata, Symphony; Siemens Medical Solutions, Erlangen, Germany) and torso phased-array coils (eight elements [Sonata and Symphony systems] or 12 elements [Avanto system]). Gradient strengths were 33 (Symphony), 40 (Sonata), and 45 mT/m (Avanto).

Implication for Patient Care

- DW imaging could potentially improve care of patients with cancer and cirrhosis by improving liver lesion detection over that achieved with standard breath-hold T2-weighted imaging.

Published online before print
10.1148/radiol.2463070432

Radiology 2008; 246:812–822

Abbreviations:
ADC = apparent diffusion coefficient
DW = diffusion weighted
FLL = focal liver lesion
GRAPPA = generalized autocalibrating partially parallel acquisition
HCC = hepatocellular carcinoma

Author contributions:
Guarantors of integrity of entire study, T.P., S.J.D., J.S.B., B.T.; study concepts/study design or data acquisition or data analysis/interpretation, all authors; manuscript drafting or manuscript revision for important intellectual content, all authors; manuscript final version approval, all authors; literature research, all authors; clinical studies, T.P., S.J.D., S.W., J.S.B., B.T.; statistical analysis, T.P., S.W., J.S.B., B.T.; and manuscript editing, T.P., V.S.L., E.M.H., J.S.B., B.T.

Authors stated no financial relationship to disclose.

DW MR imaging.—Breath-hold (n = 30) or respiratory-triggered (with a navigator-echo technique [23]) (n = 23) fat-suppressed single-shot echo-planar DW imaging was performed in the transverse plane with tridirectional diffusion gradients by using three b values (0, 50 [for FLL detection], and 500 [for FLL characterization] sec/mm^2) within the same acquisition. Parallel imaging with generalized autocalibrating partially parallel acquisition (GRAPPA) with an acceleration factor of two was applied to improve image quality (24). The other parameters were as follows: repetition time msec/echo time msec, 1300–1400/67–82; matrix, 144 × 192; section thickness, 7 mm; intersection gap, 1.4 mm; field of view, 300–400 mm with 80% rectangular field of view; number of signals acquired, two (breath hold) to four (respiratory triggered); acquisition time, less than 25 seconds for breath-hold acquisition and 120 seconds or more for respiratory-triggered acquisition.

T2-weighted MR imaging.—Transverse breath-hold T2-weighted images were obtained by using a fast short inversion time inversion-recovery sequence (TurboSTIR; Sonata and Symphony systems) (n = 29) or by using a fat-suppressed fast spin-echo T2-weighted sequence (Avanto system) (n = 24). The following parameters were used for the fast short inversion time inversion-recovery sequence: 3620–4350/85; inversion time, 150 msec; matrix, 174 × 256; section thickness, 8 mm; intersection gap, 2 mm; number of signals acquired, one; parallel imaging (GRAPPA with acceleration factor of two); echo train length, 29; echo spacing, 5 msec; 20–30 sections; and acquisition time, 36 seconds (in two concatenations). The following parameters were used for the fat-suppressed fast spin-echo T2-weighted sequence: 3570/101; matrix, 192 × 256; section thickness, 8 mm; intersection gap, 1.6 mm; 20–30 sections; one signal acquired; parallel imaging (GRAPPA with acceleration factor of two); echo train length, 29; echo spacing, 5 msec; and acquisition time, 18 seconds. In our institution, we routinely use breath-hold TurboSTIR or fast spin-echo T2-weighted imaging, which have been shown to be equal or superior to respiratory-triggered T2-weighted imaging for FLL detection in several prior studies (25–32).

In- and out-of-phase T1-weighted gradient-recalled-echo sequence.—Transverse breath-hold in- and out-of-phase T1-weighted images were obtained by using the following parameters: 126/2.3 (out of phase)–4.6 (in phase); flip angle, 80°; matrix, 179 × 256; section thickness, 8 mm; intersection gap, 2.5 mm; and one signal acquired.

Dynamic T1-weighted MR imaging.—All patients were imaged by using a transverse breath-hold three-dimensional T1-weighted fat-suppressed spoiled gradient-recalled-echo sequence (volumetric interpolated breath-hold examination) before and after dynamic injection of 20 mL of gadopentetate dimeglumine (Magnevist; Berlex Laboratories, Wayne, NJ) followed by a 20-mL saline flush (2 mL/sec) with a power injector (Spectris; Medrad, Pittsburgh, Pa). At least three time points were used: arterial, portal venous, and equilibrium phases. To determine the timing for the hepatic arterial phase, a 1-mL test bolus of contrast material was administered to determine the time to peak arterial enhancement. Portal venous and equilibrium phase imaging was performed 60 and 180 seconds, respectively, after the administration of contrast material. Acquisition parameters were as follows: 3.3–4.5/1.4–1.9; flip angle, 12°; one signal acquired; matrix, 128–192 interpolated to 256 × 256; field of view, 300–400 mm, with 80% rectangular field of view; interpolated section thickness, 2–3 mm; and slab thickness, 160–200 mm to ensure full coverage of the liver.

Image Analysis

Independent evaluation of DW and T2-weighted images.—Two observers (observer 1 [T.P.] and observer 2 [S.J.D.], each with 2 years of experience in MR imaging) retrospectively and independently reviewed DW images and T2-weighted images on a commercial workstation (Syngo; Siemens Medical Solutions). The observers were blinded to clinical MR imaging reports, clinical history, and pathologic results. DW images and T2-weighted images were randomly analyzed in two different sessions separated by at least 3 weeks to minimize recall bias. T2-weighted and DW data sets were read separately, and, as such, T2-weighted data sets were not accessed when reading DW data sets and vice versa.

Lesion detection.—For FLL detection with DW imaging, the two observers used images with b values of 0 and 50 sec/mm^2. The low b-value images are similar to T2-weighted black-blood images (18,22). The observers were asked to record only FLLs with a diameter of 1 cm or larger (because of the limited spatial resolution of DW images). Detected lesions were recorded on a data sheet on which diagrams of liver anatomy (with Couinaud segments delineated), lesion size, image number, and corresponding liver segment were noted for DW imaging and T2-weighted imaging. A maximum number of 10 FLLs per patient were recorded on the basis of the largest size. Each reader circled the 10 largest lesions and saved the digital images on the workstation. These images were used during the consensus evaluation (see below).

Lesion characterization.—The observers were asked to characterize detected lesions as benign or malignant, and they were not asked to specifically diagnose each type of FLL. Lesion characterization was performed by using a three-point scale (a score of 1 indicated benign; a score of 2, indeterminate; a score of 3, malignant) by using images with b values of 0 and 500 sec/mm^2 on the basis of lesion morphology, signal intensity, degree of signal intensity decrease with increasing b values, and qualitative assessment of ADC maps (11,14,15) (Fig 1). More specifically, the following criteria were used: A lesion was considered benign (mostly cyst and hemangioma) if the lesion was hyperintense on T2-weighted images and on DW images at b = 0 sec/mm^2 (33,34), with a strong signal intensity decrease at b = 500 sec/mm^2 and an ADC that was subjectively higher than

that of the liver (15). A lesion was considered malignant (mostly metastasis or HCC) if the lesion was mildly to moderately hyperintense on T2-weighted images (35–37) and on DW images at b = 0 sec/mm^2 and remained hyperintense compared with liver parenchyma at b = 500 sec/mm^2, with an ADC qualitatively lower than that of the surrounding liver (15). A lesion was considered indeterminate if the above criteria were not met (eg, if there was a partial signal intensity decrease or isointense ADC).

Consensus evaluation and reference standard.—The standard of reference for FLL detection and characterization was represented by the consensus reading of the two observers (T.P. and S.J.D.), which was performed 8 weeks after the initial interpretation of DW and T2-weighted images and included T2-weighted precontrast in- and out-of-phase images and dynamic postcontrast images. All FLLs detected by the two observers were reviewed by comparing the liver maps saved during the independent review with those at the consensus review. The standard of reference was represented by typical MR imaging findings and was confirmed by relevant clinical history, pathologic findings, angiographic findings, and follow-up MR imaging results. Benign lesions (cysts, hemangiomas, focal nodular hyperplasia, and adenomas) were diagnosed by using validated criteria (33,34,38–40) and by their stable appearance at follow-up MR imaging. HCC and metastases were diagnosed on the basis of clinical history; MR imaging findings, including enhancement characteristics (35–37); pathologic findings (10 patients); typical angiographic findings demonstrating arterial-phase enhancement of the tumors before transarterial chemoembolization (41,42) (13 patients with HCC); and follow-up imaging results showing interval progression (nine patients).

ADC measurement.—Pixel-based ADC maps were obtained on a commercial workstation (Syngo). ADC was calculated with a linear regression analysis of the function $S = S_0 \cdot \exp(-b \cdot \text{ADC})$, where S is the signal intensity after application of the diffusion gradient and S_0 is the signal intensity at b = 0 sec/mm^2. Three b values (0, 50, and 500 sec/mm^2) were used for ADC calculation. After the consensus reading, observer 1 measured the mean ADC of each FLL detected during consensus evaluation by drawing a region of interest over the lesion. If the lesion was larger than 3 cm, ADC was measured twice and the two measurements were averaged. To ensure that the same areas were measured, regions of interest were copied and pasted from DW images to ADC maps. For lesions not visualized on DW images, the location was determined by using postcontrast T1-weighted images.

Figure 1

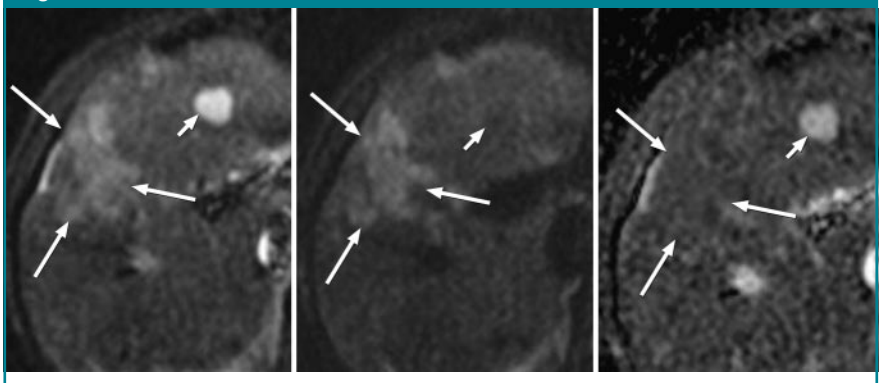

Figure 1: MR images in 55-year-old woman with metastatic breast cancer treated with chemotherapy. Transverse single-shot echo-planar DW images at b = 0 sec/mm^2 (left) and b = 500 sec/mm^2 (middle) and ADC map (right) show metastatic lesion (long arrows) and cyst (short arrows). Metastatic lesion demonstrates restricted diffusion: It is mildly hyperintense at b = 0 sec/mm^2 and remains hyperintense at b = 500 sec/mm^2, with low ADC. Cyst demonstrates free diffusion: It is hyperintense at b = 0 sec/mm^2 and hypointense at b = 500 sec/mm^2, with high ADC.

Statistical Analysis

Software (SAS, version 9.0, 2002; SAS Institute, Cary, NC) was used for analysis. Generalized estimating equations based on a binary logistic regression model were used to compare sequences (DW imaging, T2-weighted imaging) with respect to the percentage of FLLs that were detected by the two observers (detection rate) and the percentage of times each FLL was correctly characterized as benign or malignant. A separate analysis was conducted for each of the two end points—detection rate and lesion characterization. In each case, the logistic regression model included observer identification, sequence type (T2-weighted imaging vs DW imaging), and the reference standard assessment of each lesion (benign vs malignant) as classification factors and terms representing the interaction of a sequence with each observer. The analysis was performed to assess whether any difference between sequences was stronger for one observer than the other and to test whether the difference between sequences depended on whether the lesion was benign or malignant. The covariance structure was modeled by assuming observations to be correlated or independent if derived for the same patient or different patients, respectively, with the strength of correlation dependent on whether or not the observations were of the same lesion.

The detection rate of lesions stratified by location (right lobe vs left lobe) was compared between DW and T2-weighted images. Short inversion time inversion-recovery versus fat-suppressed fast spin-echo T2-weighted imaging and breath-hold versus respiratory-triggered DW imaging were compared in terms of detection rate. Only detected FLLs were evaluated for characterization for statistical analysis. An FLL that was characterized as indeterminate was classified as an incorrect characterization, irrespective of the reference standard assessment for that lesion. Short inver-

sion time inversion-recovery and fat-suppressed fast spin-echo T2-weighted imaging were compared in terms of FLL characterization.

Simple κ coefficients were used to assess interobserver agreement for lesion detection and characterization (0.00–0.20 indicated slight agreement; 0.21–0.40, fair agreement; 0.41–0.60, moderate agreement; 0.61–0.80, substantial agreement; and 0.81–1.00, almost perfect agreement) (43). The size of missed and indeterminate lesions on DW images versus T2-weighted images was compared by using a χ^2 test. Binary logistic regression and receiver operating characteristic curve analyses were conducted to evaluate the utility of the ADC measures for the prediction of malignancy. All reported *P* values are type-3 Wald significance levels and were declared to indicate a significant difference if less than .05.

Results

Consensus Reading

Overall, 211 lesions (136 malignant and 75 benign FLLs) with an average diameter of 2.8 cm (range, 1.0–15.1 cm) were detected at the consensus reading (Fig 2). There was an average of four FLLs per patient. Among the 53 included patients, there were 22 with 77 HCCs (including two completely necrotic HCCs after chemoembolization), 10 with 59 metastatic lesions, and 21 with 75 benign lesions (37 cysts in 14 patients, 23 hemangiomas in 10 patients, five adenomas in two patients, five liver abscesses in one patient, four cases of focal nodular hyperplasia in four patients, and one posttransplantation intrahepatic hematoma in one patient). Two patients with chronic hepatitis had benign FLL without HCC, and three patients with primary malignancy had benign FLL without metastatic involvement of the liver. Five patients had HCC and benign FLL, and two patients had liver metastases and benign lesions.

The diagnosis of FLL was confirmed with pathologic findings in 12 patients: six HCCs (six patients), four metastatic lesions (four patients), one intrahepatic hematoma, one adenoma, and one biliary hamartoma. In 13 additional patients with cirrhosis, the diagnosis of HCC was based on typical angiographic findings before transarterial chemoembolization (41,42). In the remaining nine patients with malignant FLLs, the diagnosis of malignancy was based on follow-up MR imaging results that demonstrated interval progression (mean follow-up time, 318 days; range, 85–467 days). The diagnosis of a benign FLL was based on typical MR imaging findings (33,34,38–40), except for the three patients described above with pathologic confirmation. The patient with liver abscesses had complete resolution of lesions after drainage and medical treatment. All five adenomas had intravoxel fat present at in- and out-of-phase imaging. There were 125 lesions in the right liver lobe, 83 in the left liver lobe, and three bridging the two liver lobes.

Figure 2

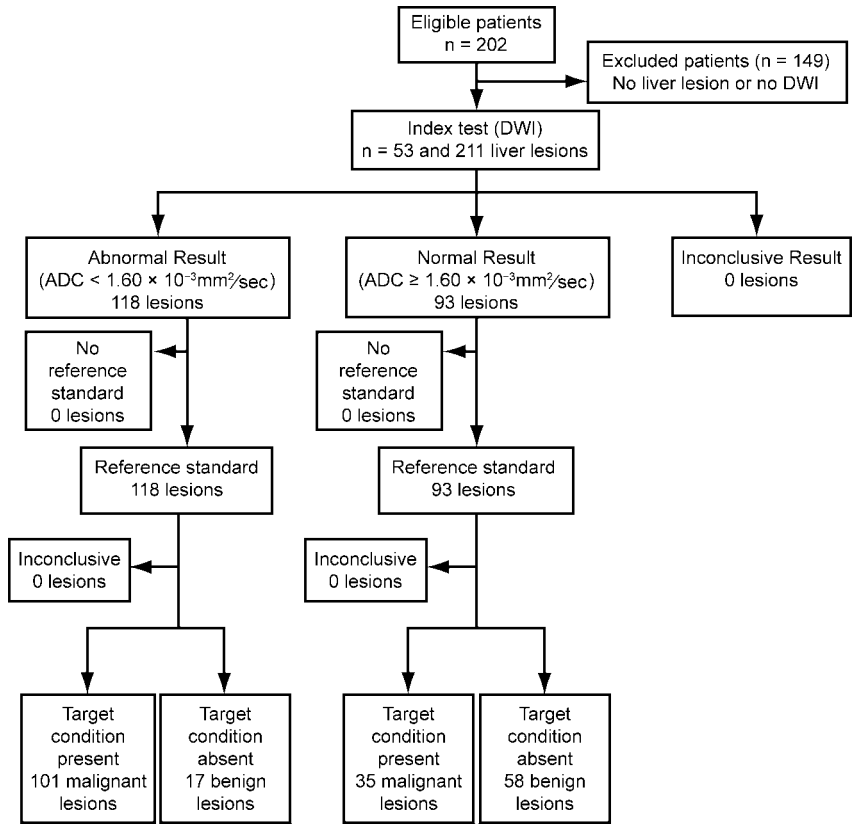

Figure 2: Flowchart shows patient population, index test results (ADC measured with DW MR imaging) for diagnosis of malignant FLLs, and reference standard.

Lesion Detection

There was no significant interaction between observer and sequence ($P = .40$) and no significant difference between observers ($P = .38$). For both observers, DW imaging was associated with a significantly higher detection rate of both malignant and benign FLLs (Table 1, Figs 3–6). When the detection performance of both observers was averaged, the number of malignant FLLs detected with DW imaging (117.5 of 136 [86.4%]) was significantly greater than that detected with T2-weighted imaging (85.5 of 136 [62.9%]) ($P < .001$).

Stratification according to malignant lesion size.—When detection rate was stratified according to malignant lesion size, there was a significant difference

only for detection of malignant FLLs with a diameter of 1–3 cm and no significant difference between DW imaging and T2-weighted imaging for lesions 3 cm in diameter or larger (Table 2). For example, DW imaging depicted significantly more malignant lesions with a diameter between 1 and 2 cm than standard T2-weighted imaging (78.5% vs 45.8%) ($P <$ .001). On average, 15.5 malignant lesions with a diameter between 1 and 2 cm were missed at DW imaging, compared with 39 missed at T2-weighted imaging.

Stratification by lesion location.—DW imaging was significantly better than T2-weighted imaging in terms of detection for both lobes (Table E1, *http://radiology.rsnajnls.org/cgi/content/full/2463070432/DC1*). There was no significant difference for detection rate with DW imaging between right and left liver lobes (88.4% and 86.1%, respectively); however, T2-weighted imaging was significantly better at detection in the right lobe than in the left lobe (75.2% and 61.4%, respectively).

Stratification by sequence.—There was no significant difference between short inversion time inversion-recovery (average between the two observers, 86.5 of 126 [68.6%]) and fat-suppressed fast spin-echo T2-weighted imaging (61.5 of 85 [72.3%]) with respect to detection rate (P = .658). On the other hand, respiratory-triggered DW imaging had a significantly higher detection rate than breath-hold DW imaging (74 of 79 [93.7%] vs 110.5 of 131 [84.3%]) (P = .032). Breath-hold DW imaging was still superior to T2-weighted imaging in terms of lesion detection ($P <$ .035).

Table 1

Detection Rate of FLLs in 53 Patients with DW and T2-weighted MR Imaging

Parameter	All Lesions (n = 211)	Malignant Lesions (n = 136)	Benign Lesions (n = 75)
DW imaging	87.7 (185/211)	86.4 (117.5/136)	90.0 (67.5/75)
T2-weighted imaging	70.1 (148/211)	62.9 (85.5/136)	83.3 (62.5/75)
P value	<.001	<.001	<.03

Note.—Data are averaged for two independent observers. Unless otherwise indicated, numbers are percentages, with raw data in parentheses.

Figure 3

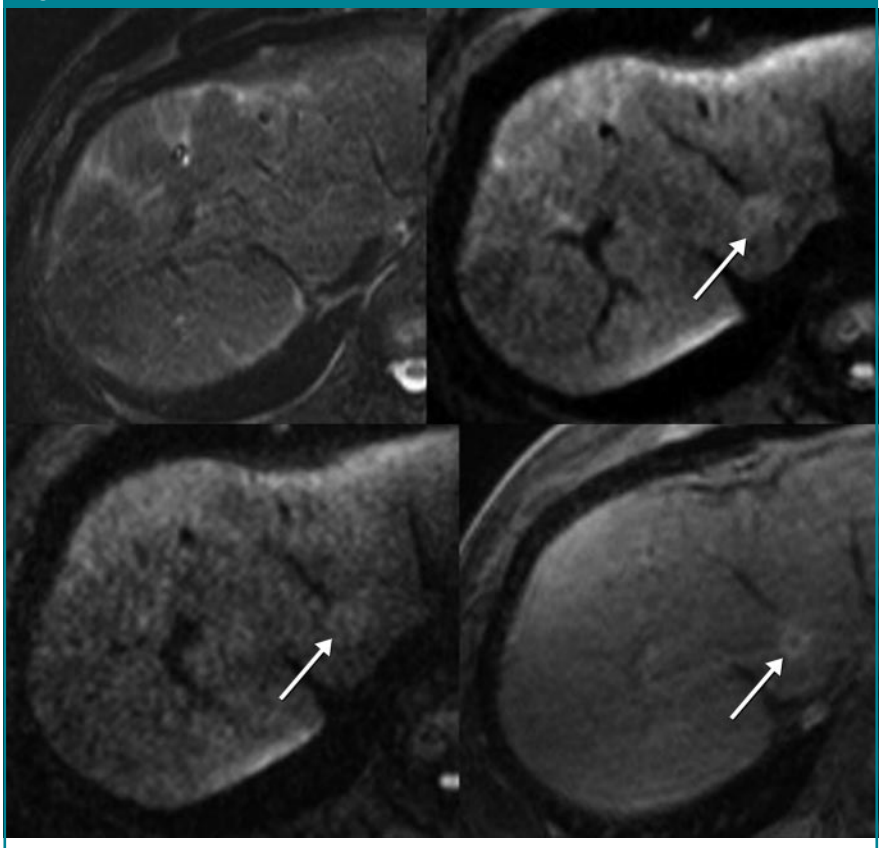

Figure 3: MR images in 68-year-old man with liver cirrhosis and small HCC in caudate lobe. Small HCC (arrows) was not visualized on transverse fat-suppressed fast spin-echo T2-weighted image (upper left) but was identified on transverse single-shot echo-planar DW image at $b = 50$ sec/mm^2 (upper right) and was hyperintense at $b = 500$ sec/mm^2 (lower left), compatible with a malignant lesion. Transverse postcontrast T1-weighted image (lower right) confirms arterial-phase enhancing lesion that is compatible with HCC.

Missed FLLs

There was no significant difference in size between lesions missed at DW imaging versus those missed at T2-weighted imaging for both observers (P = .61 for observer 1 and 0.65 for observer 2) (Table E2, *http://radiology.rsnajnls.org/cgi/content/full/2463070432/DC1*).

DW imaging.—Missed FLLs on DW images included 13 HCCs (in nine patients), two metastatic lesions (in two patients), and seven benign lesions (in seven patients: two cysts, two cases of focal nodular hyperplasia, one hemangioma, one abscess, and one adenoma) for observer 1 and 17 HCCs (in 10 patients), five metastatic lesions (in four patients), and eight benign lesions (in eight patients: three cysts, three cases of focal nodular hyperplasia, one hemangioma, and one adenoma) for observer 2. The majority (16 of 21 [76.2%]) of FLLs missed by both observers were isointense on DW images at b = 0 and b = 50 sec/mm^2. Eight FLLs (eight of 21 [38.1%]) that were missed at the initial reading by both observers were retrospectively identified

Figure 4

Figure 4: MR images in 69-year-old man with liver cirrhosis and HCC. Transverse fast short inversion time inversion-recovery (left), single-shot echo-planar DW ($b = 50$ sec/mm^2) (middle), and T1-weighted postcontrast (right) images show HCC (long arrows) in right lobe that appears mildly hyperintense on T2-weighted and DW images and hypervascular. DW and T1-weighted postcontrast images show additional small lesion (short arrows) in segment III that is not seen on T2-weighted image.

at the consensus reading. FLLs detected on DW images included all lesions detected on T2-weighted images, except for four (observer 1) and six FLLs (observer 2).

T2-weighted imaging.—Missed FLLs on T2-weighted images included 35 HCCs (in 14 patients), 15 metastatic lesions (in five patients), and 12 benign lesions (in 12 patients: six cysts, four cases of focal nodular hyperplasia, one abscess, and one adenoma) for observer 1 and 36 HCCs (in 14 patients), 15 metastatic lesions (in five patients), and 13 benign lesions (in 13 patients: five cysts, four cases of focal nodular hyperplasia, one abscess, two hemangiomas, and one adenoma) for observer 2. More than half (29 of 57 [50.9%]) of the FLLs missed by both observers were isointense on T2-weighted images. Thirty FLLs (30 of 57 [52.6%]) that were missed at the initial reading by both observers were retrospectively identified at the consensus reading.

Lesion Characterization

Both observers had similar characterization accuracy with both sequences ($P = .88$). The overall accuracy of DW images (165 of 185 [89.1%]) was slightly better than that of T2-weighted images (128.5 of 148 [86.8%]), but this was not a significant difference ($P = .51$) (Table 3). In addition, there was no statistically significant improvement with DW images compared with T2-weighted images for the evaluation of benign and malignant FLLs. Overall,

Figure 5

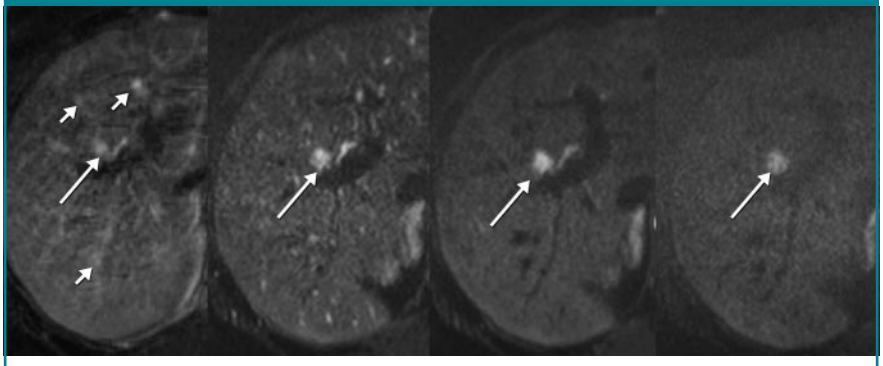

Figure 5: MR images in 62-year-old woman with metastatic colon cancer. Transverse fat-suppressed fast spin-echo T2-weighted image (left) shows several areas of T2 hyperintensity (long and short arrows), adjacent to portal vessels, that are questionable for liver lesions. Single-shot echo-planar DW images at $b = 0$ sec/mm^2 (second image from left) and $b = 50$ sec/mm^2 (third image from left) demonstrate only one lesion (arrows). Other areas of hyperintensity are vessels suppressed by small diffusion gradients, as seen on postcontrast images (not shown). Persistent hyperintensity at $b = 500$ sec/mm^2 on DW image (right) demonstrates the malignant nature of this lesion.

Figure 6

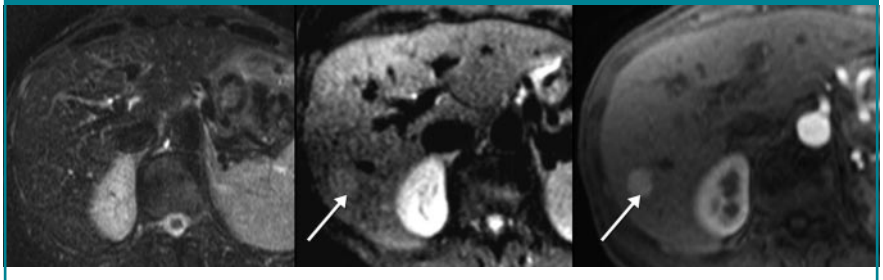

Figure 6: MR images in 59-year-old woman with focal nodular hyperplasia (arrows) of right liver lobe. Hyperplasia was not conspicuous on transverse fat-suppressed fast spin-echo T2-weighted image (left) and was detected on transverse single-shot echo-planar DW image at $b = 50$ sec/mm^2 (middle). Transverse postcontrast T1-weighted image in arterial phase (right) demonstrates early enhancement of lesion.

both T2-weighted and DW images were more accurate ($P = .04$) in the characterization of malignant FLLs (93.5 of 100.5 [93.0%]) than of benign FLLs (42 of 53 [79.2%]). There was no significant difference between short inversion time inversion-recovery (average between two observers, 72.5 of 86.5 [83.8%]) versus fat-suppressed fast spin-echo T2-weighted (55 of 61.5 [89.4%]) ($P = .48$) sequences in terms of lesion characterization.

Indeterminate FLLs

Indeterminate lesions identified on DW images were generally smaller than those identified on T2-weighted images; however, the difference was significant only for observer 2 ($P < .02$) (Table E2, *http://radiology.rsnajnls.org/cgi/content/full/2463070432/DC1*).

DW images.—There were 10 and 11 indeterminate FLLs for observers 1 and 2, respectively. For observer 1, these included four HCCs, four liver abscesses, one metastatic lesion, and one case of focal nodular hyperplasia (in six patients). For observer 2, these included three HCCs, five liver abscesses, two metastatic lesions, and one hemangioma (in six patients).

T2-weighted images.—There were nine and 12 indeterminate FLLs, respectively, for observers 1 and 2. For observer 1, these included three HCCs, three cysts, two hemangiomas, and one intrahepatic hematoma (in six patients). For observer 2, these included seven HCCs, three cysts, one metastatic lesion, and one intrahepatic hematoma (in nine patients).

Interobserver Agreement

There was substantial to almost perfect agreement both for FLL detection (Cohen $\kappa = 0.832$ for the pooled data, 0.764 for DW imaging, and 0.842 for T2-weighted imaging) and for characterization (Cohen $\kappa = 0.800$ for the pooled data, 0.772 for T2-weighted imaging, and 0.913 for DW imaging).

ADC Values

ADC values were obtained for all 211 lesions detected at consensus reading. Mean ADC values of malignant lesions were significantly lower than those of benign lesions: 1.39×10^{-3} mm^2/sec $\pm$ 0.38 (standard deviation) versus 2.19×10^{-3} mm^2/sec $\pm$ 0.67, respectively ($P < .001$), with overlap (Fig 7). The mean distribution of lesion ADCs was as follows: cysts, 2.54×10^{-3} mm^2/sec $\pm$ 0.67; hemangiomas, 2.04×10^{-3} mm^2/sec $\pm$ 0.42; liver abscesses, 1.64×10^{-3} mm^2/sec $\pm$ 0.05; focal nodular hyperplasia and adenomas, 1.49×10^{-3} mm^2/sec $\pm$ 0.49; liver metastases, 1.50×10^{-3} mm^2/sec $\pm$ 0.42; and HCCs, 1.31×10^{-3} mm^2/sec $\pm$ 0.33. The calculated area under the receiver operating characteristic curve for diagnosis of malignancy was 0.839 (95% confidence interval: 0.812, 0.863), with sensitivity of 74.2% (101 of 136), specificity of 77.3% (58 of 75), positive predictive value of 85.5% (101 of 118), negative predictive value of 62.3% (58 of 93), and accuracy of 75.3% (159 of 211), by using a threshold ADC of less than 1.60×10^{-3} mm^2/sec.

Table 2

Detection Rate in 32 Patients of 136 Malignant FLLs Stratified by Type and Size

	Lesion Type		Lesion Diameter (cm)		
Parameter	HCC ($n = 77$)	Metastatic Lesion ($n = 59$)	1–2 ($n = 72$)	2–3 ($n = 20$)	≥3 ($n = 44$)
DW imaging	80.5 (62/77)	94.0 (55.5/59)	78.5 (56.5/72)	97.5 (19.5/20)	94.3 (41.5/44)
T2-weighted imaging	53.9 (41.5/77)	74.6 (44/59)	45.8 (33/72)	75.0 (15/20)	85.2 (37.5/44)
P value	<.001	.025	<.001	.034	.096

Note.—Data are averaged for two independent observers. Unless otherwise indicated, numbers are percentages, with raw data in parentheses.

Table 3

Correctly Characterized FLLs with DW and T2-weighted MR Imaging

Parameter	All Lesions ($n = 211$)	Benign Lesions ($n = 75$)	Malignant Lesions ($n = 136$)
DW imaging	89.1 (165/185)	83.0 (56/67.5)	92.3 (108.5/117.5)
T2-weighted imaging	86.8 (128.5/148)	80.0 (50/62.5)	91.8 (78.5/85.5)
P value	.51	.33	.60

Note.—Data are averaged for two independent observers. Unless otherwise indicated, numbers are percentages, with raw data in parentheses.

Discussion

Our study results showed significantly improved detection rates of both malignant and benign FLLs when using DW imaging with a small *b* value compared with standard breath-hold T2-weighted imaging, particularly for small malignant lesions measuring 1–3 cm. Our study results also demonstrated equivalent detection of lesions located in the right versus left lobe at DW imaging and poorer performance of T2-weighted imaging for detection of FLLs located in the left lobe. In addition, respiratory-triggered DW imaging (with a navigator echo) was better for detection than breath-hold DW imaging (in that only five lesions were missed). We showed equivalent performance of DW imaging and T2-weighted imaging for FLL characterization. Better FLL detection with DW imaging by using a small *b* value (50 sec/mm^2) is attributed to suppression of background vessels, equivalent to that achieved with black-blood images, with better contrast-to-noise ratio and better lesion conspicuity.

Despite significant differences in detection of benign and malignant FLLs on a group basis, characterization of FLLs by using ADCs showed overlap, with

sensitivity and specificity for diagnosis of malignant lesions lower than what we described previously (15) owing to a different lesion distribution. Most prior studies (8–17) have used DW imaging for FLL characterization, and there are limited data on the use of DW imaging for FLL detection (18–20,22). Only two of these studies (18,22) involved a direct comparison of DW imaging and T2-weighted imaging by using small *b* values (20–188 sec/mm^2). In 48 patients with 49 FLLs, Okada et al (18) showed better detection of metastatic lesions with DW imaging (with a *b* value of 55 sec/mm^2) than with T2-weighted imaging. Hussain et al (22) (who used a *b* value of 20 sec/mm^2) demonstrated that DW imaging can be optimized by combining parallel imaging, decreased frequency encoding points, and small diffusion gradients to achieve image quality and signal-to-noise ratio similar to those of T2-weighted imaging. Although we did not measure contrast-to-noise ratio of DW imaging and T2-weighted imaging, it was shown previously to be generally improved by using small *b* values (17,18,22), potentially improving lesion detection. Moteki and Sekine (19) demonstrated higher liver-to-lesion signal intensity ratios with small diffusion gradients for HCC and metastatic lesions compared with images without diffusion gradient, with improved detection of a small number of liver lesions (three metastatic lesions and six HCCs) and worsened detection of two HCCs. To our knowledge, prior to our study, there were no studies on the evaluation of detection and characterization of FLLs by using DW imaging and comparing that with standard breath-hold T2-weighted imaging. The improved detection of FLLs that measure 1–3 cm with DW imaging is one of the important findings in our study and a potential emerging application of DW imaging.

While results of a study by Nasu et al (20) have shown increased detection of metastatic lesions with a combination of DW imaging and precontrast T1- and T2-weighted imaging (82%) compared with pre- and postcontrast (superparamagnetic iron oxide) imaging (66%), and results of another recently published study (21) have demonstrated added detection of tumor foci with DW imaging compared with that with conventional sequences (pre- and postcontrast imaging), the potential benefit of DW imaging in association or compared with conventional gadolinium-enhanced liver MR imaging remains to be investigated.

T2-weighted imaging is helpful in the diagnosis of FLLs in the noncirrhotic and cirrhotic liver (26,35,44–48), and standard T2-weighted imaging sequences are part of routine liver MR imaging protocols. Results of several studies (25–27,29–32) have demonstrated the equivalent or better performance of breath-hold T2-weighted imaging compared with respiratory-triggered T2-weighted imaging in terms of image quality and FLL detection and characterization, with a much shorter acquisition time. Many centers (including ours) have been routinely using breath-hold T2-weighted imaging for liver imaging. Limitations of T2-weighted imaging include difficulty in differentiation of vessels from lesions, limited detection of small liver lesions, and image artifacts in patients with ascites. For example, results of two prior studies (49,50) have shown the limited role of T2-weighted imaging in the detection and characterization of HCC in cirrhosis, mostly related to HCC signal intensity on T2-weighted images, appearing iso- or hypointense in 42.1%–53% of HCCs. It is possible that the heterogeneity and increased signal intensity of the cirrhotic liver parenchyma as a result of nodular regeneration, fibrosis, and scarring obscures the mildly hyperintense HCC nodules on T2-weighted images (51,52). Our study results confirm that T2-weighted imaging is poor for HCC detection, with improved detection by using DW imaging. On DW images, we found much higher contrast between HCC and cirrhotic liver than on T2-weighted images. One potential explanation is the possible associated iron deposition seen in Kupffer cells and hepatocytes in cirrhotic liver that can cause T2* shortening, which results in increased lesion-to-liver contrast on echo-planar images (53,54).

Figure 7

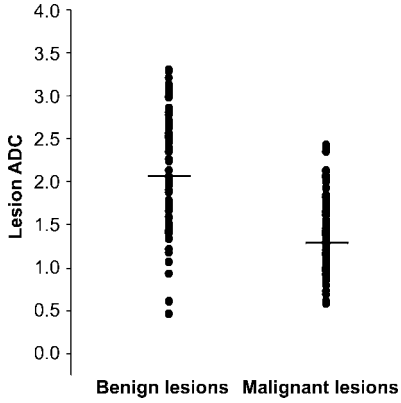

Figure 7: Scatterplot shows distribution of ADC values of 211 focal liver lesions. There was a significant difference in mean ADC between benign ($n = 75$) and malignant ($n = 136$) lesions: 2.19×10^{-3} mm^2/sec $\pm$ 0.67 and 1.39×10^{-3} mm^2/sec $\pm$ 0.38, respectively ($P < .001$). Bars = mean ADC values.

Our study had limitations. First, the T2-weighted data set included a combination of short inversion time inversion-recovery and fat-suppressed fast spin-echo images that have slightly different image contrasts. We used this combination because we prefer the robust fat suppression and the insensitivity to magnetic field inhomogeneity of the short inversion time inversion-recovery method with certain imagers at our institution. However, we did not find differences between the two sequences in terms of FLL detection and characterization. Second, the DW data set included a combination of breath-hold and respiratory-triggered images that have different signal-to-noise ratio and image quality. However, despite the superiority of respiratory-triggered DW imaging over breath-hold DW imaging for lesion detection, breath-hold DW imaging still was better than T2-weighted imaging for lesion detection. Third, pathologic diagnosis was not available for most patients and/or lesions. Fourth, the same observers were used for the reference standard evaluation and for the initial interpretations, potentially leading to bias. Fifth, the patient population did not include patients without FLLs. This precluded our ability to assess false-negative findings.

In conclusion, our study results show improved detection of malignant and benign FLLs by using DW imaging compared with standard breath-hold T2-weighted imaging, with equivalent performance of DW imaging and T2-weighted imaging for lesion characterization.

References

1. Jamison RL, Donohue JH, Nagorney DM, Rosen CB, Harmsen WS, Ilstrup DM. Hepatic resection for metastatic colorectal cancer results in cure for some patients. Arch Surg 1997;132:505–511.
2. Mazzaferro V, Regalia E, Doci R, et al. Liver transplantation for the treatment of small hepatocellular carcinomas in patients with cirrhosis. N Engl J Med 1996;334:693–699.
3. Heslin MJ, Medina-Franco H, Parker M, Vickers SM, Aldrete J, Urist MM. Colorectal hepatic metastases: resection, local ablation, and hepatic artery infusion pump are associated with prolonged survival. Arch Surg 2001;136:318–323.
4. Llovet JM, Bruix J. Systematic review of randomized trials for unresectable hepatocellular carcinoma: chemoembolization improves survival. Hepatology 2003;37:429–442.
5. Hussain SM, Semelka RC, Mitchell DG. MR imaging of hepatocellular carcinoma. Magn Reson Imaging Clin N Am 2002;10:31–52, v.
6. Pedro MS, Semelka RC, Braga L. MR imaging of hepatic metastases. Magn Reson Imaging Clin N Am 2002;10:15–29.
7. Motohara T, Semelka RC, Nagase L. MR imaging of benign hepatic tumors. Magn Reson Imaging Clin N Am 2002;10:1–14.
8. Muller MF, Prasad P, Siewert B, Nissenbaum MA, Raptopoulos V, Edelman RR. Abdominal diffusion mapping with use of a whole-body echo-planar system. Radiology 1994;190:475–478.
9. Moteki T, Ishizaka H, Horikoshi H, Matsumoto M. Differentiation between hemangiomas and hepatocellular carcinomas with the apparent diffusion coefficient calculated from turboFLASH MR images. J Magn Reson Imaging 1995;5:187–191.
10. Namimoto T, Yamashita Y, Sumi S, Tang Y, Takahashi M. Focal liver masses: characterization with diffusion-weighted echo-planar MR imaging. Radiology 1997;204:739–744.
11. Ichikawa T, Haradome H, Hachiya J, Nitatori T, Araki T. Diffusion-weighted MR imaging with a single-shot echoplanar sequence: detection and characterization of focal hepatic lesions. AJR Am J Roentgenol 1998; 170:397–402.
12. Ichikawa T, Haradome H, Hachiya J, Nitatori T, Araki T. Diffusion-weighted MR imaging with single-shot echo-planar imaging in the upper abdomen: preliminary clinical experience in 61 patients. Abdom Imaging 1999;24:456–461.
13. Yamada I, Aung W, Himeno Y, Nakagawa T, Shibuya H. Diffusion coefficients in abdominal organs and hepatic lesions: evaluation with intravoxel incoherent motion echo-planar MR imaging. Radiology 1999;210:617–623.
14. Kim T, Murakami T, Takahashi S, Hori M, Tsuda K, Nakamura H. Diffusion-weighted single-shot echoplanar MR imaging for liver disease. AJR Am J Roentgenol 1999;173: 393–398.
15. Taouli B, Vilgrain V, Dumont E, Daire JL, Fan B, Menu Y. Evaluation of liver diffusion isotropy and characterization of focal hepatic lesions with two single-shot echo-planar MR imaging sequences: prospective study in 66 patients. Radiology 2003;226: 71–78.
16. Yoshikawa T, Kawamitsu H, Mitchell DG, et al. ADC measurement of abdominal organs and lesions using parallel imaging technique. AJR Am J Roentgenol 2006;187:1521–1530.
17. Moteki T, Horikoshi H. Evaluation of hepatic lesions and hepatic parenchyma using diffusion-weighted echo-planar MR with three values of gradient b-factor. J Magn Reson Imaging 2006;24:637–645.
18. Okada Y, Ohtomo K, Kiryu S, Sasaki Y. Breath-hold T2-weighted MRI of hepatic tumors: value of echo planar imaging with diffusion-sensitizing gradient. J Comput Assist Tomogr 1998;22:364–371.
19. Moteki T, Sekine T. Echo planar MR imaging of the liver: comparison of images with and without motion probing gradients. J Magn Reson Imaging 2004;19:82–90.
20. Nasu K, Kuroki Y, Nawano S, et al. Hepatic metastases: diffusion-weighted sensitivity-encoding versus SPIO-enhanced MR imaging. Radiology 2006;239:122–130.
21. Low RN, Gurney J. Diffusion-weighted MRI (DWI) in the oncology patient: value of breathhold DWI compared to unenhanced and gadolinium-enhanced MRI. J Magn Reson Imaging 2007;25:848–858.
22. Hussain SM, De Becker J, Hop WC, Dwarkasing S, Wielopolski PA. Can a single-shot black-blood T2-weighted spin-echo echo-planar imaging sequence with sensitivity encoding replace the respiratory-triggered turbo spin-echo sequence for the liver? an optimization and feasibility study. J Magn Reson Imaging 2005;21:219–229.
23. Asbach P, Klessen C, Kroencke TJ, et al. Magnetic resonance cholangiopancreatography using a free-breathing T2-weighted turbo spin-echo sequence with navigator-triggered prospective acquisition correction. Magn Reson Imaging 2005;23:939–945.
24. Taouli B, Martin AJ, Qayyum A, et al. Parallel imaging and diffusion tensor imaging for diffusion-weighted MRI of the liver: preliminary experience in healthy volunteers. AJR Am J Roentgenol 2004;183:677–680.
25. Rydberg JN, Lomas DJ, Coakley KJ, Hough DM, Ehman RL, Riederer SJ. Comparison of breath-hold fast spin-echo and conventional spin-echo pulse sequences for T2-weighted MR imaging of liver lesions. Radiology 1995; 194:431–437.
26. Soyer P, de Givry SC, Gueye C, Lenormand S, Somveille E, Scherrer A. Detection of focal hepatic lesions with MR imaging: prospective comparison of T2-weighted fast spin-echo with and without fat suppression, T2-weighted breath-hold fast spin-echo, and gadolinium chelate-enhanced 3D gradient-recalled imaging. AJR Am J Roentgenol 1996;166:1115–1121.
27. Kim TK, Wang WC, Han JK, Cho SG, Choi BI. T2-weighted MR imaging for hepatic hemangiomas: comparison of breath-hold and non-breath-hold turbo spin-echo pulse sequences with phased-array multicoil. Abdom Imaging 1998;23:422–426.
28. Earls JP, Rofsky NM, DeCorato DR, Krinsky GA, Weinreb JC. Echo-train STIR MRI of the liver: comparison of breath-hold and non-breath-hold imaging strategies. J Magn Reson Imaging 1999;9:87–92.
29. Katayama M, Masui T, Kobayashi S, et al. Fat-suppressed T2-weighted MRI of the liver: comparison of respiratory-triggered fast spin-echo, breath-hold single-shot fast spin-echo, and breath-hold fast-recovery fast spin-echo sequences. J Magn Reson Imaging 2001;14:439–449.
30. Augui J, Vignaux O, Argaud C, Coste J, Gouya H, Legmann P. Liver: T2-weighted MR imaging with breath-hold fast-recovery optimized fast spin-echo compared with breath-hold half-Fourier and non-breath-hold respiratory-triggered fast spin-echo pulse sequences. Radiology 2002;223:853–859.
31. Huang J, Raman SS, Vuong N, Sayre JW, Lu DS. Utility of breath-hold fast-recovery fast spin-echo t2 versus respiratory-triggered fast spin-echo T2 in clinical hepatic imaging. AJR Am J Roentgenol 2005;184:842–846.
32. Akin O, Schwartz LH, Welber A, Maier CF,

Decorato DR, Panicek DM. Evaluation of focal liver lesions: fast-recovery fast spin echo T2-weighted MR imaging. Clin Imaging 2006;30:322–325.

33. Semelka RC, Brown ED, Ascher SM, et al. Hepatic hemangiomas: a multi-institutional study of appearance on T2-weighted and serial gadolinium-enhanced gradient-echo MR images. Radiology 1994;192:401–406.

34. Hussain SM, Terkivatan T, Zondervan PE, et al. Focal nodular hyperplasia: findings at state-of-the-art MR imaging, US, CT, and pathologic analysis. RadioGraphics 2004;24:3–17.

35. Earls JP, Theise ND, Weinreb JC, et al. Dysplastic nodules and hepatocellular carcinoma: thin-section MR imaging of explanted cirrhotic livers with pathologic correlation. Radiology 1996;201:207–214.

36. Krinsky GA, Lee VS, Theise ND, et al. Hepatocellular carcinoma and dysplastic nodules in patients with cirrhosis: prospective diagnosis with MR imaging and explantation correlation. Radiology 2001;219:445–454.

37. Danet IM, Semelka RC, Leonardou P, et al. Spectrum of MRI appearances of untreated metastases of the liver. AJR Am J Roentgenol 2003;181:809–817.

38. Vilgrain V, Flejou JF, Arrive L, et al. Focal nodular hyperplasia of the liver: MR imaging and pathologic correlation in 37 patients. Radiology 1992;184:699–703.

39. Arrive L, Flejou JF, Vilgrain V, et al. Hepatic adenoma: MR findings in 51 pathologically proved lesions. Radiology 1994;193:507–512.

40. Mortele KJ, Praet M, Van Vlierberghe H, de Hemptinne B, Zou K, Ros PR. Focal nodular hyperplasia of the liver: detection and characterization with plain and dynamic-enhanced MRI. Abdom Imaging 2002;27:700–707.

41. Bartolozzi C, Lencioni R, Caramella D, Palla A, Bassi AM, Di Candio G. Small hepatocellular carcinoma: detection with US, CT, MR imaging DSA, and Lipiodol-CT. Acta Radiol 1996;37:69–74.

42. Krinsky GA, Nguyen MT, Lee VS, et al. Dysplastic nodules and hepatocellular carcinoma: sensitivity of digital subtraction hepatic arteriography with whole liver explant correlation. J Comput Assist Tomogr 2000;24:628–634.

43. Landis JR, Koch GG. An application of hierarchical kappa-type statistics in the assessment of majority agreement among multiple observers. Biometrics 1977;33:363–374.

44. Kadoya M, Matsui O, Takashima T, Nonomura A. Hepatocellular carcinoma: correlation of MR imaging and histopathologic findings. Radiology 1992;183:819–825.

45. Semelka RC, Shoenut JP, Kroeker MA, et al. Focal liver disease: comparison of dynamic contrast-enhanced CT and T2-weighted fat-suppressed, FLASH, and dynamic gadolinium-enhanced MR imaging at 1.5 T. Radiology 1992;184:687–694.

46. Low RN, Francis IR, Sigeti JS, Foo TK. Abdominal MR imaging: comparison of T2-weighted fast and conventional spin-echo, and contrast-enhanced fast multiplanar spoiled gradient-recalled imaging. Radiology 1993;186:803–811.

47. Soyer P, Gouhiri M, Rondeau Y, Spelle L, Mosnier H, Scherrer A. Non-breath-hold fast spin-echo versus breath-hold fast spin-echo and spoiled gradient-recalled echo MR imaging in the detection of hepatic tumors: correlation with surgical findings. AJR Am J Roentgenol 1997;168:1199–1204.

48. Pawluk RS, Tummala S, Brown JJ, Borrello JA. A retrospective analysis of the accuracy of T2-weighted images and dynamic gadolinium-enhanced sequences in the detection and characterization of focal hepatic lesions. J Magn Reson Imaging 1999;9:266–273.

49. Hussain HK, Syed I, Nghiem HV, et al. T2-weighted MR imaging in the assessment of cirrhotic liver. Radiology 2004;230:637–644.

50. Hecht EM, Holland AE, Israel GM, et al. Hepatocellular carcinoma in the cirrhotic liver: gadolinium-enhanced 3D T1-weighted MR imaging as a stand-alone sequence for diagnosis. Radiology 2006;239:438–447.

51. Marti-Bonmati L, Talens A, del Olmo J, et al. Chronic hepatitis and cirrhosis: evaluation by means of MR imaging with histologic correlation. Radiology 1993;188:37–43.

52. Semelka RC, Chung JJ, Hussain SM, Marcos HB, Woosley JT. Chronic hepatitis: correlation of early patchy and late linear enhancement patterns on gadolinium-enhanced MR images with histopathology initial experience. J Magn Reson Imaging 2001;13:385–391.

53. Krinsky GA, Lee VS, Nguyen MT, et al. Siderotic nodules in the cirrhotic liver at MR imaging with explant correlation: no increased frequency of dysplastic nodules and hepatocellular carcinoma. Radiology 2001;218:47–53.

54. Krinsky GA, Lee VS, Nguyen MT, et al. Siderotic nodules at MR imaging: regenerative or dysplastic? J Comput Assist Tomogr 2000;24:773–776.